

X-Distill: Cross-Architecture Vision Distillation for Visuomotor Learning

Maanping Shao[#], Feihong Zhang[#], Gu Zhang, Baiye Cheng, Zhengrong Xue, Huazhe Xu[†]

[#]Equal contribution [†]Corresponding author X-Distill.github.io

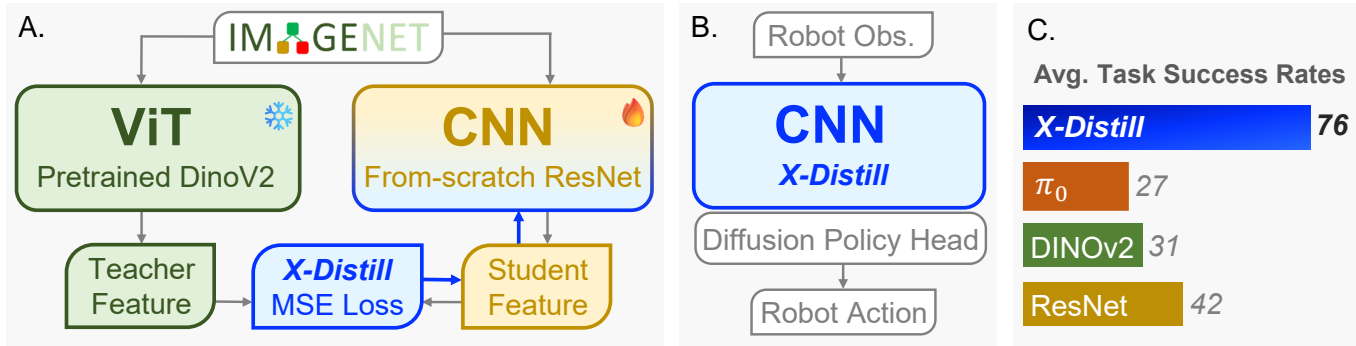


Fig. 1: **X-Distill** is a simple yet effective visual encoder enabling data-efficient visuomotor learning. **A.** X-Distill is obtained by cross-architecture knowledge distillation from a large ViT teacher into a compact CNN student on general-purpose image datasets. **B.** Designed for visuomotor policy learning, X-Distill can be jointly fine-tuned end-to-end with a diffusion policy head on robotics-specific datasets. **C.** Given a few ($20 \sim 25$) demonstrations per task, X-Distill significantly outperforms representative counterparts on real-world manipulation tasks, exhibiting its surprising effectiveness.

Abstract—Visuomotor policies often leverage large pre-trained Vision Transformers (ViTs) for their powerful generalization capabilities. However, their significant data requirements present a major challenge in the data-scarce context of most robotic learning settings, where compact CNNs with strong inductive biases can be more easily optimized. To address this trade-off, we introduce X-Distill, a simple yet highly effective method that synergizes the strengths of both architectures. Our approach involves an offline, cross-architecture knowledge distillation, transferring the rich visual representations of a large, frozen DINOv2 teacher to a compact ResNet-18 student on the general-purpose ImageNet dataset. This distilled encoder, now endowed with powerful visual priors, is then jointly fine-tuned with a diffusion policy head on the target manipulation tasks. Extensive experiments on 34 simulated benchmarks and 5 challenging real-world tasks demonstrate that our method consistently outperforms policies equipped with from-scratch ResNet or fine-tuned DINOv2 encoders. Notably, X-Distill also surpasses 3D encoders that utilize privileged point cloud observations or much larger Vision-Language Models. Our work highlights the efficacy of a simple, well-founded distillation strategy for achieving state-of-the-art performance in data-efficient robotic manipulation.

Index Terms—Visuomotor Policy, Knowledge Distillation, Representation Learning, Manipulation

This work was supported by Institute for Interdisciplinary Information Sciences, Tsinghua University, Shanghai Qi Zhi Institute and Shanghai Artificial Intelligence Laboratory.(*Maanping Shao and Feihong Zhang are co-first authors, contributed equally to this work.*)(Corresponding author: Huazhe Xu.)

Maanping Shao, Feihong Zhang, Gu Zhang and Zhengrong Xue are with Tsinghua University, Beijing 100084, China.(email:smap24@mails.tsinghua.edu.cn, zf24@mails.tsinghua.edu.cn, zg24@mails.tsinghua.edu.cn, xzf23@mails.tsinghua.edu.cn)

Baiye Cheng is with Huazhong University of Science and Technology, Wuhan 430074, China.(email:U202212594@hust.edu.cn)

Huazhe Xu is with the Institute for Interdisciplinary Information Sciences, Tsinghua University, Beijing 100084, China, and also with Shanghai Qi Zhi Institute, Shanghai 200030, China, as well as with Shanghai Artificial Intelligence Laboratory, Shanghai 200032, China.(email: huazhe_xu@mails.tsinghua.edu.cn)

I. INTRODUCTION

VISUOMOTOR policies, exemplified by Diffusion Policy [1], are promising solutions for generalizable robotic manipulation. As end-to-end approaches, they typically rely on a visual encoder to extract manipulation-centric features from the raw pixels of a scene, followed by a policy head that generates concrete robot actions conditioning on the extracted visual features.

Benefiting from the success of large-scale vision pre-training [2], [3], it has become a common practice in recent advances [4], [5] to initialize the visual encoder in a visuomotor policy with off-the-shelf, pre-trained Vision Transformers (ViTs) [6], e.g., CLIP [3] or DINOv2 [7]. These ViT-backend pre-trained models are found to exhibit enhanced generalization capabilities compared to Convolutional Neural Network (CNN) counterparts lacking open-world semantic knowledge, e.g., a ResNet [8] trained from scratch.

However, lacking the strong intrinsic inductive biases inherent to CNNs, such as locality and translation equivariance, ViTs are known to struggle when faced with limited amounts of training data [6], [9]. This issue becomes prominent and inevitable in the context of robot learning, where the dataset size is significantly smaller than in computer vision. Despite the recent trend among embodied AI startups to train policies with hundreds of *hours* of high-quality data produced by a data collection factory [10]–[12], most researchers in academia typically collect data by hand, thus favoring data-efficient policies that perform well under a dataset size constraint of tens to a few hundred manipulation *trajectories*.

In this work, we find that simple advances to the visual encoder can yield higher-performing and more data-efficient visuomotor policies. More specifically, we design a cross-architecture vision distillation mechanism, or **X-Distill** in

short, which attempts to combine the merits of both the open-world semantic generalization capabilities of pre-trained ViT models, and the inductive bias of CNN architectures that facilitate policy optimization under the low-data regime.

On an implementation level, we instantiate X-Distill by selecting DINOv2 (ViT-L/14) as the teacher encoder, a lightweight from-scratch ResNet-18 as the student encoder, and the mean squared error (MSE) between the teacher and student features as the knowledge distillation [13] loss. To make the X-Distilled encoder generally effective for diverse tasks, environments, and robot platforms, we choose the general-purpose ImageNet dataset as the distillation corpus, avoiding potential overfitting to any specific robotic scenarios. After X-Distillation, the CNN-backend encoder with ViT pre-training knowledge can be seamlessly integrated into the policy learning pipeline, jointly fine-tuned with the policy head in an end-to-end manner on any robotics-specific datasets.

We validate the effectiveness of X-Distill by conducting experiments on 34 simulated tasks across MetaWorld [14], Adroit [15], [16], and DexArt [17] benchmarks, with 10 demonstrations per task. We also design 5 real-world tasks, carefully defining their In-Distribution (ID) and Out-of-Distribution (OOD) conditions and preparing 20 ~ 25 demonstrations per task. Empirically, we find that Diffusion Policy with X-Distill consistently outperforms counterparts equipped with ResNet from scratch or DINOv2 as the encoder. Additionally, our policy also outperforms 3D Diffusion Policy [18], which utilizes privileged 3D observation, as well as π_0 [10], a Vision-Language-Action (VLA) model that adopts a much larger VLM [19] as the visual perception encoder. Finally, we present a detailed qualitative analysis of the learned representations, providing insights into how X-Distill achieves superior performance over the baseline methods. ***Please refer to the project website for robot videos.***

II. RELATED WORKS

A. Visual Representation Learning

After the dominance of Convolutional Neural Networks (CNNs) [8], [20] in the 2010s, Vision Transformers (ViTs) [6], [9] have gained increasing popularity in the 2020s because of their superior scaling capabilities and impressive representational power when pre-trained on large-scale datasets [2], [21]. Despite this trend, CNNs maintain a crucial edge in low-data regimes and continue to see widespread practical deployment. The key reason is their strong **inductive bias** — the convolutional operator imposes assumptions of locality and spatial weight sharing, which make them remarkably data-efficient. On the other hand, ViTs lack such biases and therefore require exposure to massive datasets to learn fundamental visual concepts. This discrepancy in data requirements keeps CNNs popular in many specialized domains, such as medical diagnostics [22] or manufacturing quality control [23], where large labeled datasets are often unavailable.

B. Cross-Architecture Knowledge Distillation

Knowledge distillation (KD) has become a cornerstone technique for model compression and knowledge transfer. Most work has focused on distillation between **homologous architectures**, including traditional CNN-to-CNN approaches [13]

and more modern ViT-to-ViT frameworks designed for efficiency such as TinyViT [24]. For robotics, homologous knowledge distillation was recently explored by Theia [25], which fuses knowledge from multiple pre-trained ViTs into a single unified ViT encoder. In comparison, **cross-architecture distillation** is comparatively underexplored. [26]. A representative work is DeiT [9], a CNN-to-ViT distillation where a CNN teacher can stabilize a data-hungry ViT student. By contrast, our work adopts the converse approach: a ViT-to-CNN distillation aiming to combine the inductive bias of a CNN with the powerful semantic understanding of a large-scale pre-trained ViT.

C. Visuomotor Policy Learning

Visuomotor policy learning is a promising paradigm for robotic manipulation. Representative works in this vein include Diffusion Policy [1] and related approaches [27]–[29], which typically consists of a visual encoder followed by a policy head network. Recently, Vision-Language-Action (VLA) models have been proposed to replace the visual encoder with more capable vision-language models (VLMs) [10], [30], enabling impressive generalization abilities such as zero-shot skill deployment in unseen homes [31]. However, finetuning the VLM requires a substantial amount of training data. State-of-the-art VLAs such as π_0 [10], AgiBot GO-1 [11], and Galaxea G0 [12] all rely on their embodiment-specific large-scale datasets, measured either in millions by the number of trajectories or in hundreds of hours by the physical on-robot execution time. In this work, we focus on training capable visuomotor policies when a limited amount of training data is available, i.e., using only ~ 25 demonstration trajectories per task.

III. METHOD

This section details the X-Distill framework, whose overall procedure is summarized in Algorithm 1.

A. X-Distill: A Cross-Architecture Distillation Method

We employ cross-architecture knowledge distillation to transfer the representational capabilities of a large Vision Transformer (ViT) into a compact CNN with beneficial inductive biases. Crucially, this entire process is conducted exclusively on the general-purpose ImageNet-1K [32] dataset (\mathcal{X}), which contains approximately 1.3 million images depicting a wide variety of real-world objects and scenes. This decoupling of visual feature distillation from the downstream domain-specific datasets makes X-Distill entirely **domain-agnostic**. In other words, the resulting X-Distill encoder is universally suitable for all kinds of robotic manipulation tasks, thus avoiding potential overfitting to any specific environments, camera setups, or robotic embodiments.

a) Selection of teacher and student networks.: We select the pre-trained DINOv2 (ViT-L/14) model as our teacher \mathcal{T} . With approximately 304M parameters, this large-scale model is used off-the-shelf as a frozen feature extractor, serving as a robust source of semantic and structural visual knowledge. For the student model \mathcal{S} , we choose a highly compact ResNet-18 architecture with only 11M parameters. The choice of student

Algorithm 1 How to acquire and leverage X-Distill.

```

1: Step 1: Knowledge Distillation
2: Input: Teacher encoder  $\mathcal{T}$  (frozen DINOv2), Student encoder  $\mathcal{S}$  (from-scratch ResNet), Domain-agnostic dataset  $\mathcal{D}_{\text{large}}$  (ImageNet).
3: for each training epoch do
4:   for each batch  $x \in \mathcal{D}_{\text{large}}$  do
5:      $z_T \leftarrow f_{\mathcal{T}}(x)$ .
6:      $z_S \leftarrow f_{\mathcal{S}}(x)$ .
7:      $L \leftarrow \mathcal{L}_{\text{KD}}(z_S, \text{sg}(z_T))$  # Eq. (1)
8:     Update student encoder  $\mathcal{S}$  via  $\nabla_{\mathcal{S}} L$ .
9:   end for
10: end for
11: Save the weights of  $\mathcal{S}$  as  $\mathcal{S}^*$ 
12: Output: X-Distilled encoder weights  $\mathcal{S}^*$ .
1: Step 2: Policy Finetuning
2: Input: X-Distilled encoder weights  $\mathcal{S}^*$ , Diffusion policy head  $\pi_{\theta}$ , Domain-specific dataset  $\mathcal{D}_{\text{robotics}}$ .
3: Initialize encoder  $\mathcal{S}$  with weights from  $\mathcal{S}^*$ .
4: for each training epoch do
5:   for each batch  $(o, a) \in \mathcal{D}_{\text{robotics}}$  do
6:      $z_{\text{img}} \leftarrow f_{\mathcal{S}}(x)$ .
7:      $c \leftarrow \text{concat}(z_{\text{img}}, s)$ .
8:     Compute  $L_{\text{diff}}$ . # Eq. (2)
9:     Update  $\mathcal{S}$  and  $\pi_{\theta}$  via  $\nabla_{\mathcal{S}, \theta} L_{\text{diff}}$ .
10:  end for
11: end for
12: Output: Trained encoder and policy  $(\mathcal{S}^{**}, \pi_{\theta}^*)$ .
```

network prioritizes not only its computational efficiency with a network parameter size nearly $28\times$ smaller than the teacher, but also its strong inductive biases such as spatial locality that are beneficial for manipulation tasks.

b) Domain-agnostic distillation.: The student is trained to replicate the feature outputs of the teacher on ImageNet-1K. For a given input image x , we extract the global [CLS] token from the DINOv2 teacher, which serves as the target feature vector. The ResNet-18 student architecture is modified with a final linear layer to match the feature dimension of the teacher. The core objective is then to minimize the direct Mean Squared Error (MSE) between these two feature vectors:

$$\mathcal{L}_{\text{KD}} = \mathbb{E}_{x \sim \mathcal{X}} \left[\|f_{\mathcal{T}}(x) - f_{\mathcal{S}}(x)\|_2^2 \right] \quad (1)$$

where $f_{\mathcal{T}}$ and $f_{\mathcal{S}}$ represent the complete feature extraction processes of the teacher and the dimension-aligned student, respectively. This process results in a ResNet-18 with parameter weights \mathcal{S}^* , which encodes the open-world generalization knowledge of the teacher network.

B. Finetuning X-Distill for Visuomotor Policy Learning

Given the powerful initialization provided by X-Distill, we deploy the encoder \mathcal{S}^* for downstream policy learning on a target robotics dataset. We use a Diffusion Policy [1] head, which generates action chunks conditioned on robot observations.

At each timestep, the distilled encoder \mathcal{S}^* processes a history of camera images $x_{t-T_o+1:t}$ into a visual feature vector z_{img} . This vector is concatenated with the robot's

proprioceptive state s_t to form a comprehensive conditioning vector, $c = \text{concat}(z_{\text{img}}, s_t)$. This conditioning vector c guides the entire action generation process. During inference, actions are generated by iteratively denoising a random Gaussian tensor, conditioned on this vector c .

Crucially, both the distilled encoder \mathcal{S}^* and the diffusion policy head π_{θ} are jointly trained on robotics-specific datasets. This end-to-end optimization allows the powerful, general-purpose features from the distillation phase to be fine-tuned and specialized for the specific demands of the manipulation task. The entire system is optimized by minimizing the diffusion loss objective:

$$\mathcal{L}_{\text{diff}} = \mathbb{E}_{\mathbf{A}^0, \epsilon, k} \left[\|\epsilon - \epsilon_{\theta}(\mathbf{A}^0 + \sigma_k \epsilon | c, k)\|^2 \right], \quad (2)$$

where \mathbf{A}^0 denotes the ground-truth actions, $\epsilon \sim \mathcal{N}(0, \mathbf{I})$, and k is sampled from the diffusion steps.

IV. SIMULATION EXPERIMENTS**A. Setup**

Simulation benchmarks. To thoroughly evaluate the effectiveness of our method, we conduct experiments across a total of 34 tasks from 3 distinct MuJoCo-based robotic manipulation benchmarks. Our evaluation encompasses tasks requiring parallel gripper manipulation from MetaWorld [14], dexterous motor skills from Adroit [15], [16], and articulated object manipulation from DexArt [17]. Tasks in MetaWorld are categorized into various difficulty levels—*easy*, *medium*, *hard*, and *very hard*—based on [33].

Expert demonstrations. 10 trajectories are collected for each simulation task. For MetaWorld, scripted policies are employed. Trajectories in the remaining domains are gathered using agents trained via reinforcement learning (RL): specifically, VRL3 [34] is applied for Adroit, while PPO [35] is utilized for the remaining benchmarks.

Evaluation Metric. We report all results averaged over 3 random seeds (0, 1, and 2). For each individual training run, we evaluate the policy on 20 episodes every 200 epochs, and the highest success rate achieved throughout the run is reported for that seed. The final values presented in our tables are the mean of these scores across the 3 seeds.

B. Performance

Compared methods. We compare X-Distilled ResNet-18 (11M) against several visual encoder counterparts with a similar number of parameters, including:

- **ResNet-scratch** [8], ResNet-18 (11M) trained from scratch;
- **DINOv2** [7], ViT-small (21M) pre-trained using large-scale self-supervision;
- **Depth-Anything** [36], ViT-small (24.8M) trained for monocular depth estimation;
- **Theia** [25], ViT-small (22M) that distills multiple vision foundation models.

Additionally, we also benchmark against **PointNet-DP3** [18], a PointNet-based architecture (0.06M) processing privileged background-cropped 3D point cloud observations.

Main results. As summarized in Table I, X-Distill achieves the best overall average performance across all 34 tasks. It consistently outperforms all 2D vision baselines by a significant margin, securing state-of-the-art success rates in most

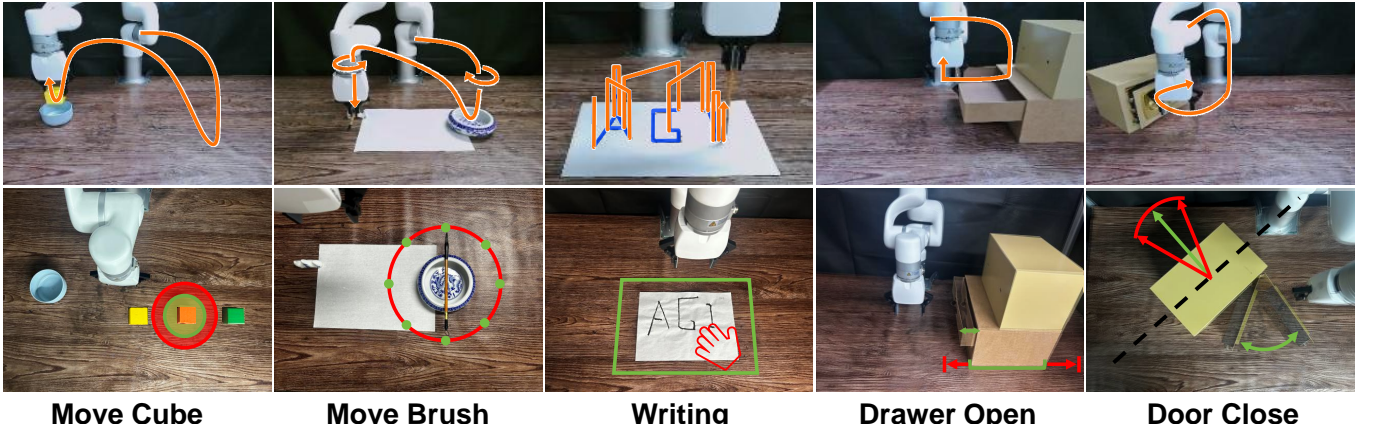


Fig. 2: **Visualization of configurations for our real-world tasks.** The orange arrow provides a schematic representation of the gripper trajectory as derived from the data. The green regions represent the distribution of object/robot configurations seen during training demonstrations, while the red regions illustrate the novel configurations used for generalization testing.

TABLE I
AVERAGED SUCCESS RATES ON METAWORLD, ADROIT AND DEXART BENCHMARKS.
 POINTNET-DP3 IS MARKED IN GRAY BECAUSE IT PROCESSES PRIVILEGED BACKGROUND-CROPPED
 3D POINT CLOUDS.

Method	MetaWorld				Adroit (3)	Dexart (2)	Average
	(easy 20)	(medium 7)	(hard 1)	(very hard 1)			
ResNet-scratch	76.6	48.0	38.0	50.0	37.7	54.5	64.1
DINOv2	78.5	46.0	48.0	38.0	51.7	58.0	66.2
Depth-Anything	68.2	29.3	42.0	43.0	40.3	66.0	56.1
Theia	50.9	13.7	0.0	38.3	8.7	24.0	36.0
X-Distill (Ours)	93.9	88.3	48.0	88.0	68.3	63.5	87.2
PointNet-DP3	90.4	70.6	14.0	72.0	40.7	85.0	84.0

TABLE II

ABLATION STUDY ON METAWORLD BENCHMARKS. WE EVALUATE THE IMPACT OF TEACHER MODEL SCALE (DINOv2-L VS. S), STUDENT ARCHITECTURAL BIAS (CNN VS. ViT), AND STUDENT MODEL SCALE.

Teacher	Student	MW-20 (easy)	MW-7 (medium)	MW-1 (hard)	MW-1 (v. hard)	Average
DINOv2-L	ResNet-18 (11M)	93.9	88.3	48.0	88.0	90.7
	ViT-S-Half (11M)	72.0	25.3	2.0	40.0	57.2
	ConvNeXt (89M)	91.8	77.4	50.0	83.0	86.6
DINOv2-S	ResNet-18 (11M)	94.3	87.3	43.0	90.0	<u>90.6</u>

simulation benchmarks. This validates the effectiveness of our distillation strategy for data-scarce visuomotor learning.

Notably, our 2D approach remains highly competitive even in geometrically demanding settings where methods leveraging privileged 3D inputs have a natural advantage. For instance, the DexArt-Toilet task requires the robot to lift the toilet lid from a frontal viewpoint, which is inherently challenging to estimate the depth relationship between the gripper and the object to be manipulated from a single RGB image. Nevertheless, X-Distill still demonstrates decent performance in many of these challenging tasks, showcasing a strong prior in spatial reasoning.

C. Ablation Studies

We conduct ablation studies to investigate the impact of the teacher network parameter size, as well as the student network architectural bias and parameter size within our X-Distill framework. The ablation results are summarized in Table II.

Teacher network parameter size. We distill **DINOv2-S** (21M) and **DINOv2-L** (304M) teachers into the same ResNet-18 student. No significant difference can be observed between DINOv2-S and DINOv2-L, indicating our X-Distill framework is insensitive to the specific network configurations of a well-pre-trained teacher network. Nevertheless, we use the DINOv2-L teacher for all subsequent experiments to ensure the maximized knowledge quality that the teacher could provide.

Student network architectural bias. We distill the same DINOv2-L teacher into a **ResNet-18** (11M) and a customized **ViT-S-Half** (11M) of the same size. The ResNet-18 student substantially outperforms its ViT counterpart by 33.5%. This highlights the crucial role of convolutional inductive biases for visuomotor learning in a low-data regime, supporting our primary hypothesis.

Student network parameter size. We compare our compact **ResNet-18** (11M) student to a much larger **ConvNeXt** (89M) [37] CNN counterpart. Despite its greater capacity, the larger model achieves a slightly degraded success rate by 4.1%

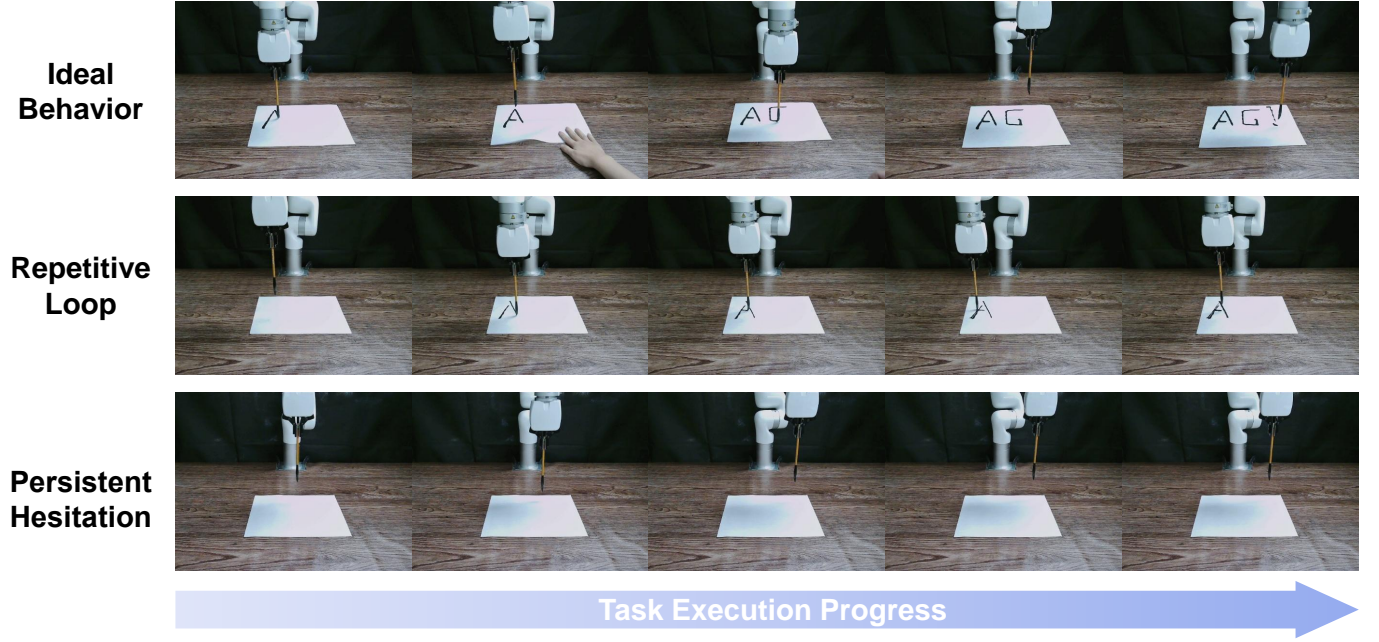


Fig. 3: **Representative trajectory types observed in the “Writing AGI” task.** We identify three distinct behaviors: (1) **Ideal Behavior:** Successful and robust execution of all three letters, even under perturbation. (2) **Repetitive Loop:** Perseverative behavior where the policy gets stuck repeatedly writing the first letter ‘A’. (3) **Persistent Hesitation:** Dithering motion above the paper without initiating the writing task.

TABLE III
A COMPARISON OF TASK EXECUTION SUCCESS RATES (%) FOR REAL-WORLD TASKS, ALONG WITH THE NUMBERS OF DEMONSTRATIONS AND EVALUATION TRIALS.

Method	Move Cube			Move Brush			Writing “AGI”		Drawer Open		Door Close		Average
	ID	OOD	C-Gen	ID	OOD	ID	OOD	ID	OOD	ID	OOD	ID	
# Demos	20	0	0	24	0	25	0	20	0	20	0	20	-
# Eval Trials	15	5	10	4	8	5	4	5	15	5	10	5	-
ResNet-scratch	66.7	0.0	50.0	0.0	0.0	40.0	25.0	100.0	13.3	60.0	80.0	41.9	
DINOv2	26.7	20.0	20.0	0.0	0.0	0.0	0.0	80.0	13.3	100.0	90.0	31.4	
π_0 (SFT)	0.0	0.0	0.0	25.0	0.0	0.0	0.0	80.0	33.3	80.0	90.0	26.7	
X-Distill (Ours)	93.3	40.0	70.0	75.0	25.0	100.0	100.0	100.0	53.3	100.0	100.0	75.6	

on robotics tasks. This confirms our intuition that smaller visual encoders with stronger inductive biases are easier to optimize, thus beneficial for data-efficient policy learning.

V. REAL-WORLD EXPERIMENTS

A. Experiment Setup

We conduct all real-world experiments with an X-Arm 6 robotic arm, capture image observations through a web camera at 15Hz, and prepare a small collection of demonstrations ($20 \sim 25$) per task via Meta-Quest VR teleoperation. We design 5 tabletop manipulation tasks, and carefully define their In-Distribution (ID) and Out-of-Distribution (OOD) object randomization ranges for rigorous and repeatable evaluation. Task execution trajectories as well as ID and OOD ranges are illustrated in Figure 2. Detailed numbers of demonstrations and evaluation trials can be found in Table III.

More specifically, **Move Cube** requires the robot to pick up an orange cube and place it into a bowl. In addition to testing

on OOD cube positions, we also conduct a color generalization (C-Gen) test with unseen yellow and green cubes. **Move Brush** requires the robot to pick up a brush pen with various initial orientational and translational offsets and place it onto a stand. **Writing “AGI”** requires the robot to sequentially write letters “AGI” on a randomly placed piece of paper. We conduct OOD dynamic perturbation trials, where human perturbators randomly drag the paper elsewhere while the robot is writing letters. **Drawer Open** requires the robot to insert its finger into varying initial gaps of the randomly placed drawer, and then open it by sliding outward. **Door Close** requires the robot to close the door from various initial open angles by pushing it inward.

B. Experiment Results and Analysis

Baselines. We compare our X-Distill encoder against three representative counterparts. The first two are Diffusion Policies equipped with either a ResNet encoder trained from scratch or an off-the-shelf DINOv2 encoder. Both of the two baseline

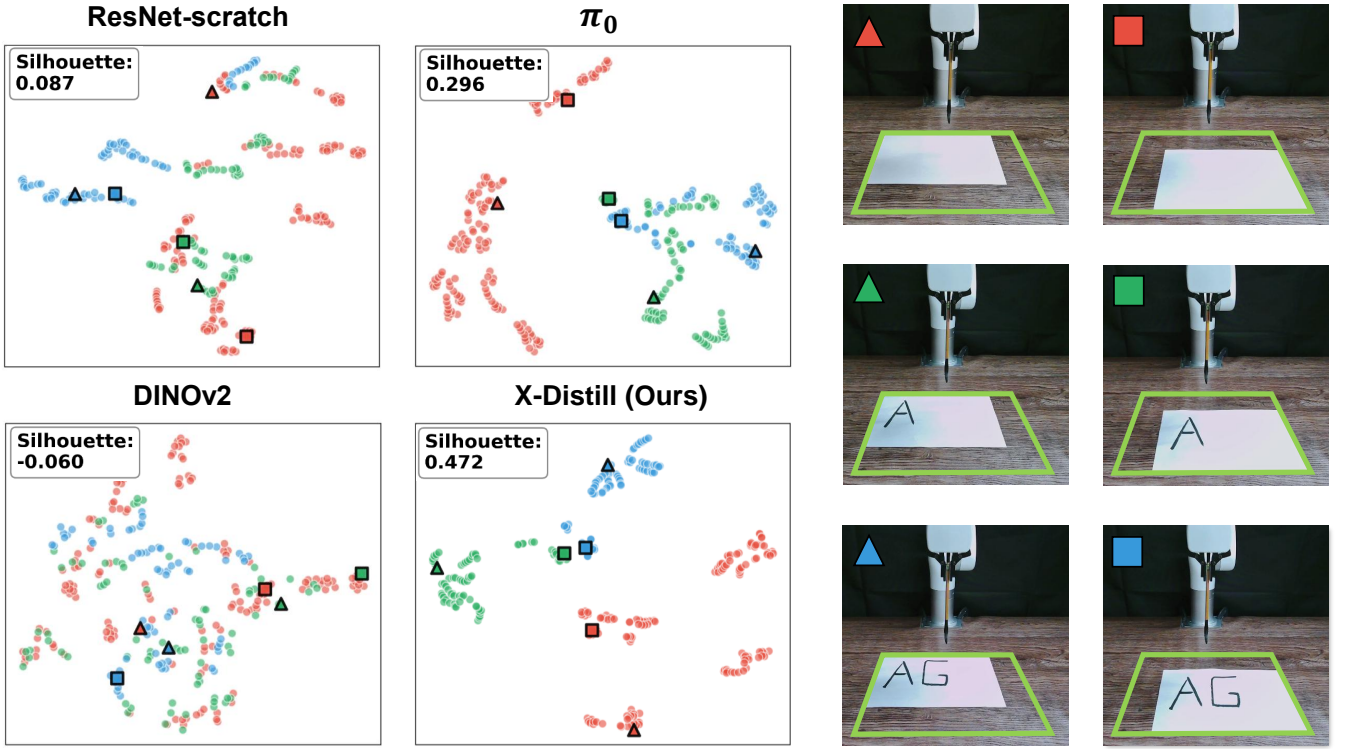


Fig. 4: t-SNE visualization of learned feature spaces on the “Writing AGI” task. Our X-Distill encoder learns to form three distinct clusters corresponding to the task’s semantic stages, quantitatively confirming a well-separated feature space with a high Silhouette Score [38] of 0.472, which indicates a high degree of cluster cohesion and separation compared with the baselines. This semantic separability is crucial for the policy to accurately identify the current task stage, enabling precise long-horizon planning for the sequential writing task.

policies, as well as our approach, are trained for 1500 epochs on our task-specific data. Our third baseline is the state-of-the-art Vision-Language-Action (VLA) model, π_0 [10]. Considering its significant computational requirements, we performed supervised fine-tuning (SFT) for 30,000 steps, following the official recommendations, which took approximately 20 hours on a single A100 GPU. All methods were trained using the same dataset consisting of the same limited number of demonstrations to ensure a fair comparison.

Main results. The quantitative results for real-world experiments are summarized in Table III. X-Distill demonstrates clear superiority, consistently outperforming all baseline approaches by a large margin and achieving the highest success rates across both ID and OOD evaluation settings. Simply finetuning a large ViT encoder like DINoV2 yields poor performance, confirming the challenge of effectively optimizing large Transformer networks in data-scarce scenarios and underscoring the effectiveness of our cross-architecture distillation.

The performance gap is particularly insightful when comparing against the VLA model, π_0 . While π_0 shows reasonable success on simpler tasks like **Drawer Open**, it struggles significantly on more complex, high-precision tasks such as **Writing “AGI”**, where its performance drops to zero. This suggests that directly finetuning a large, generalist VLA on small, task-specific datasets is a significant challenge. In contrast, our X-Distill framework effectively bridges this gap by transferring knowledge into a compact, data-efficient architecture, highlighting the importance of matching the model

and pre-training strategy to the available data resources.

C. Qualitative Analysis

We focus on our most challenging long-horizon task, **Writing “AGI”**, where success critically depends on the encoder’s ability to discern subtle but crucial visual state changes. For instance, before starting to write ‘G’, the robot’s physical state is nearly identical to when it starts writing ‘A’; the only distinguishing information is the visual context of the letter ‘A’ already present on the paper.

Empirically, we observe that Diffusion Policy with ResNet-scratch often fails by repeatedly executing the trajectory for ‘A’, indicating an inability to visually differentiate these critical semantic states. Meanwhile, Diffusion Policy with DINoV2 and π_0 (SFT) often get stuck and start trembling before writing any letter, which is a potential sign of underfitting. In comparison, Diffusion Policy with X-Distill is the only one among the compared methods that manages to differentiate all critical stages and completes writing all the three letters sequentially one by one. Even under severe external disturbances that drag the paper away during the writing process, the X-Distill-empowered policy is still robust, responsively following the movement of the paper and rapidly adapting to the correct position for writing the next letter. Example trajectories are shown in Figure 3. To provide deeper insights into how X-Distill achieves superior quantitative performance compared to its counterparts, we conduct further t-SNE analysis and saliency map visualization of the learned visual representations.

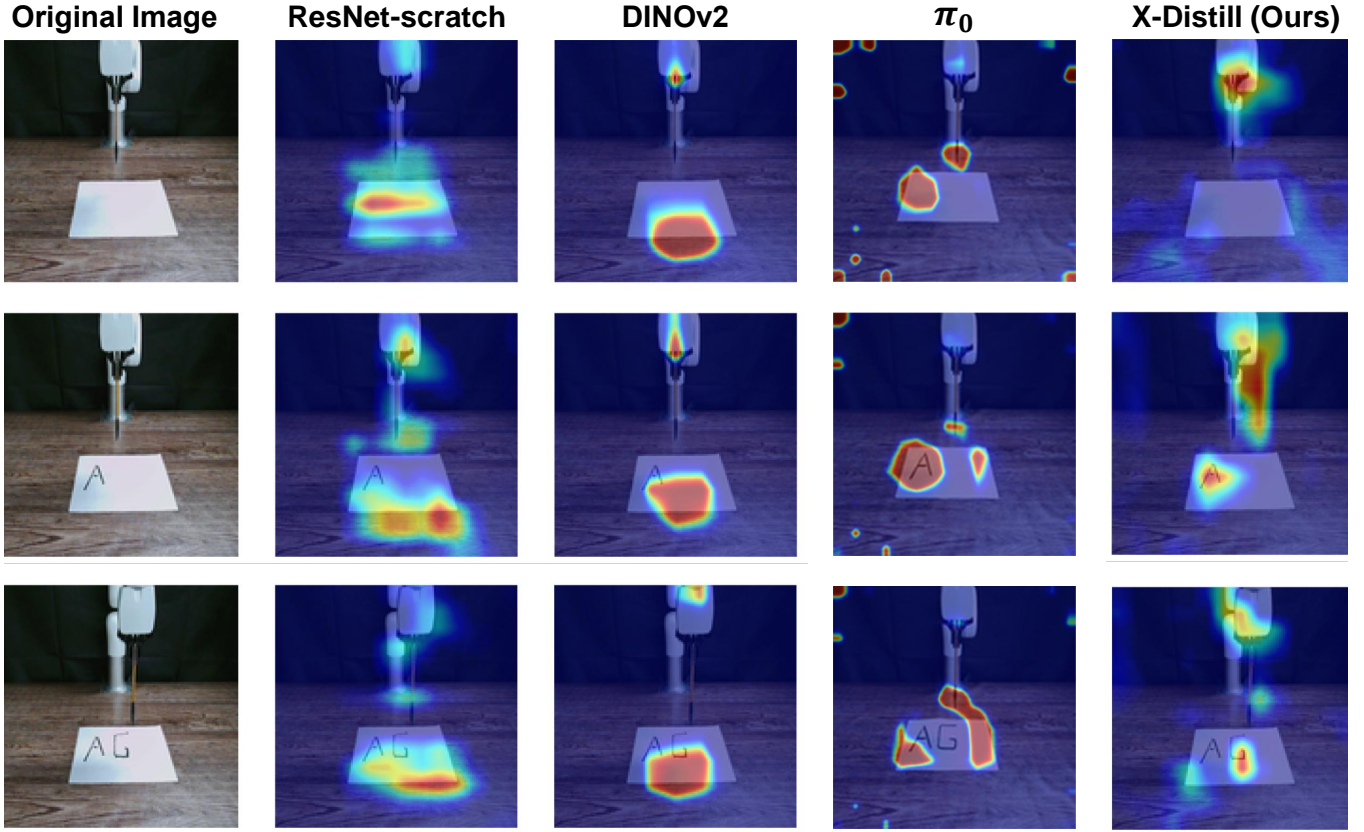


Fig. 5: **Saliency map comparison on the “Writing AGI” task.** We visualize the model’s visual focus at the beginning of each writing stage. Our X-Distill encoder correctly shifts its attention from the gripper (before ‘A’), to the letter ‘A’ (before ‘G’), and finally to the letter ‘G’ (before ‘I’). Baseline models exhibit diffuse or irrelevant attention.

t-SNE visualization of feature space separability. The global structure of the learned feature space is visualized via t-SNE [39] in Figure 4. Each data point corresponds to the feature of a frame sampled from three crucial stages for policy decision making marked in three respective colors: (1) before writing ‘A’, (2) before writing ‘G’, and (3) before writing ‘I’. The features produced from an ideal visual encoder should form three distinct clusters, corresponding to the three colors. It can be observed that X-Distill gives a more separable feature space than the Paligemma [19] encoder extracted from π_0 , while the features from both ResNet-scratch and DINOv2 are nearly indistinguishable. These results indicate that X-Distill learns a feature space that is semantically coherent and robust to visual distractors.

Inspecting task-relevant feature attribution via saliency maps. To further investigate how our X-Distill achieves emergent semantic feature separation, we inspect pixel-level feature attribution by visualizing the saliency maps. For saliency visualization, we adopt Grad-CAM for CNN-based models [40], and the cross-attention strengths between the [CLS] token and all local patch features for ViT-based models [41], [42], providing a cross-architecture comparison of the visual focus. As shown in Figure 5, both DINOv2 and π_0 are unable to effectively shift the high-attention regions throughout the task progress, which cross-verifies our earlier judgment of underfitting. Meanwhile, the saliency maps of ResNet-scratch and X-Distill exhibits more reasonable shifting patterns, but

the latter is significantly more precise. More specifically, before writing ‘A’ on the blank page, the full attention of X-Distill is focused on the **robot gripper**, the primary actor. Then, before writing ‘G’, its focus dynamically shifts to the **letter ‘A’** already on the paper. Finally, before writing ‘I’, X-Distill shifts attention again, attending to the **letter ‘G’**, whose appearance serves as the cue to write the final letter ‘I’.

The t-SNE and saliency map visualizations combined reveal that X-Distill successfully learns a semantically meaningful and robust visual representation. Such representation can well differentiate critical states and dynamically focus on task-relevant visual cues, which ultimately contributes to the policy’s success in complex long-horizon manipulation tasks.

VI. CONCLUSION

We introduced **X-Distill**, a framework addressing the trade-off between ViT generalization and CNN sample efficiency. By distilling DINOv2 features into a ResNet-18 on ImageNet, we obtain a robust encoder for data-scarce robotics. Extensive experiments on 34 simulated and 5 real-world tasks show X-Distill outperforms standard baselines and even privileged 3D or VLA policies. Our analysis attributes this to the learned semantically separable feature space. Ultimately, X-Distill demonstrates that a simple, well-founded distillation strategy is a key enabler for data-efficient visuomotor learning. We believe X-Distill provides a practical and effective pathway towards building capable visuomotor policies with limited

data, and hope it will inspire further research on cross-architecture knowledge distillation for robotics.

Limitations and Future Work. While effective, our direct feature distillation leaves room for exploration. Future directions include adopting sophisticated techniques to align intermediate features [26] and distilling from multimodal VLA teachers to incorporate language priors. Additionally, while we focus on the data-scarce regime, investigating X-Distill’s scalability in data-rich scenarios and its application to dynamic tasks like mobile manipulation remain important open questions.

REFERENCES

- [1] C. Chi, S. Feng, Y. Du, Z. Xu, E. Cousineau, B. Burchfiel, and S. Song, “Diffusion policy: Visuomotor policy learning via action diffusion,” *RSS*, 2023.
- [2] M. Caron, H. Toultron, I. Misra, H. Jégou, J. Mairal, P. Bojanowski, and A. Joulin, “Emerging properties in self-supervised vision transformers,” in *Proceedings of the IEEE/CVF international conference on computer vision*, 2021, pp. 9650–9660.
- [3] A. Radford, J. W. Kim, C. Hallacy, A. Ramesh, G. Goh, S. Agarwal, G. Sastry, A. Askell, P. Mishkin, J. Clark *et al.*, “Learning transferable visual models from natural language supervision,” *International Conference on Machine Learning (ICML)*, pp. 8748–8763, 2021.
- [4] F. Lin, Y. Hu, P. Sheng, C. Wen, J. You, and Y. Gao, “Data scaling laws in imitation learning for robotic manipulation,” *arXiv preprint arXiv:2410.18647*, 2024.
- [5] Z. Xue, S. Deng, Z. Chen, Y. Wang, Z. Yuan, and H. Xu, “Demogen: Synthetic demonstration generation for data-efficient visuomotor policy learning,” *arXiv preprint arXiv:2502.16932*, 2025.
- [6] A. Dosovitskiy, L. Beyer, A. Kolesnikov, D. Weissenborn, X. Zhai, T. Unterthiner, M. Dehghani, M. Minderer, G. Heigold, S. Gelly *et al.*, “An image is worth 16x16 words: Transformers for image recognition at scale,” in *International Conference on Learning Representations (ICLR)*, 2021.
- [7] M. Oquab, T. Dariseti, T. Moutakanni, H. Vo, M. Szafraniec, V. Khalidov, P. Fernandez, D. Haziza, F. Massa, A. El-Nouby, R. Howes, P.-Y. Huang, H. Xu, V. Sharma, S.-W. Li, W. Galuba, M. Rabbat, M. Assran, N. Ballas, G. Synnaeve, I. Misra, H. Jegou, J. Mairal, P. Labatut, A. Joulin, and P. Bojanowski, “Dinov2: Learning robust visual features without supervision,” 2023. [Online]. Available: <https://arxiv.org/abs/2304.07193>
- [8] K. He, X. Zhang, S. Ren, and J. Sun, “Deep residual learning for image recognition,” *CVPR*, 2016.
- [9] H. Toultron, M. Cord, M. Douze, F. Massa, A. Sablayrolles, and H. Jégou, “Training data-efficient image transformers & distillation through attention,” *ICML*, 2021.
- [10] K. Black, N. Brown, D. Driess, A. Esmail, M. Equi, C. Finn, N. Fusai, L. Groom, K. Hausman, B. Ichter *et al.*, “ π_0 : A vision-language-action flow model for general robot control,” *arXiv preprint arXiv:2410.24164*, 2024.
- [11] Q. Bu, J. Cai, L. Chen, X. Cui, Y. Ding, S. Feng, S. Gao, X. He, X. Hu, X. Huang *et al.*, “Agibot world colosseo: A large-scale manipulation platform for scalable and intelligent embodied systems,” *arXiv preprint arXiv:2503.06669*, 2025.
- [12] T. Jiang, T. Yuan, Y. Liu, C. Lu, J. Cui, X. Liu, S. Cheng, J. Gao, H. Xu, and H. Zhao, “Galaxea open-world dataset and g0 dual-system vla model,” *arXiv preprint arXiv:2509.00576*, 2025.
- [13] G. Hinton, O. Vinyals, and J. Dean, “Distilling the knowledge in a neural network,” *NeurIPS*, 2015.
- [14] T. Yu, D. Quillen, Z. He, R. Julian, K. Hausman, C. Finn, and S. Levine, “Meta-world: A benchmark and evaluation for multi-task and meta reinforcement learning,” in *CoRL*, 2020.
- [15] V. Kumar, “Manipulators and manipulation in high dimensional spaces,” Ph.D. dissertation, University of Washington, Seattle, 2016.
- [16] A. Rajeswaran, V. Kumar, A. Gupta, G. Vezzani, J. Schulman, E. Todorov, and S. Levine, “Learning complex dexterous manipulation with deep reinforcement learning and demonstrations,” *arXiv preprint arXiv:1709.10087*, 2017.
- [17] C. Bao, H. Xu, Y. Qin, and X. Wang, “Dexart: Benchmarking generalizable dexterous manipulation with articulated objects,” in *CVPR*, 2023.
- [18] Y. Ze, G. Zhang, K. Zhang, C. Hu, M. Wang, and H. Xu, “3d diffusion policy: Generalizable visuomotor policy learning via simple 3d representations,” *arXiv preprint arXiv:2403.03954*, 2024.
- [19] L. Beyer, A. Steiner, A. S. Pinto, A. Kolesnikov, X. Wang, D. Salz, M. Neumann, I. Alabdulmohsin, M. Tschannen, E. Bugliarello *et al.*, “Paligemma: A versatile 3b vlm for transfer,” *arXiv preprint arXiv:2407.07726*, 2024.
- [20] K. Simonyan and A. Zisserman, “Very deep convolutional networks for large-scale image recognition,” *ICLR*, 2014.
- [21] K. He, H. Fan, Y. Wu, S. Xie, and R. Girshick, “Momentum contrast for unsupervised visual representation learning,” *CVPR*, 2020.
- [22] F. Shamshad, S. Khan, S. W. Zamir, M. H. Khan, M. Hayat, F. S. Khan, and H. Fu, “Transformers in medical imaging: A survey,” *Medical image analysis*, vol. 88, p. 102802, 2023.
- [23] J. Liu, G. Xie, J. Wang, S. Li, C. Wang, F. Zheng, and Y. Jin, “Deep industrial image anomaly detection: A survey,” *Machine Intelligence Research*, vol. 21, no. 1, pp. 104–135, 2024.
- [24] K. Wu, J. Zhang, H. Peng, M. Liu, B. Xiao, J. Fu, and L. Yuan, “Tinyvit: Fast pretraining distillation for small vision transformers,” 2022. [Online]. Available: <https://arxiv.org/abs/2207.10666>
- [25] J. Shang, K. Schmeckpeper, B. B. May, M. V. Minniti, T. Kelestemur, D. Watkins, and L. Herlant, “Theia: Distilling diverse vision foundation models for robot learning,” *arXiv preprint arXiv:2407.20179*, 2024.
- [26] Y. Liu, J. Cao, B. Li, W. Hu, J. Ding, and L. Li, “Cross-architecture knowledge distillation,” 2022. [Online]. Available: <https://arxiv.org/abs/2207.05273>
- [27] T. Pearce, T. Rashid, A. Kanervisto, D. Bignell, M. Sun, R. Georgescu, S. V. Macua, S. Z. Tan, I. Momennejad, K. Hofmann *et al.*, “Imitating human behaviour with diffusion models,” *ICLR*, 2023.
- [28] M. Reuss, M. Li, X. Jia, and R. Lioutikov, “Goal-conditioned imitation learning using score-based diffusion policies,” *arXiv preprint arXiv:2304.02532*, 2023.
- [29] Z. Xian, N. Gkanatsios, T. Gervet, T.-W. Ke, and K. Fragkiadaki, “Chaineddiffuser: Unifying trajectory diffusion and keypose prediction for robotic manipulation,” in *CoRL*, 2023.
- [30] S. Reed, K. Zolna, E. Parisotto, S. Colmenarejo, A. Novikov, G. Barth-Maron, M. Gimenez, Y. Sulsky, J. Kay, J. Springenberg *et al.*, “Openvla: An open-source vision-language-action model,” *arXiv:2306.00091*, 2023.
- [31] P. Intelligence, K. Black, N. Brown, J. Darpinian, K. Dhabalia, D. Driess, A. Esmail, M. Equi, C. Finn, N. Fusai, M. Y. Galliker, D. Ghosh, L. Groom, K. Hausman, B. Ichter, S. Jakubczak, T. Jones, L. Ke, D. LeBlanc, S. Levine, A. Li-Bell, M. Mothukuri, S. Nair, K. Pertsch, A. Z. Ren, L. X. Shi, L. Smith, J. T. Springenberg, K. Stachowicz, J. Tanner, Q. Vuong, H. Walke, A. Walling, H. Wang, L. Yu, and U. Zhilinsky, “ $\pi_{0.5}$: a vision-language-action model with open-world generalization,” 2025. [Online]. Available: <https://arxiv.org/abs/2504.16054>
- [32] J. Deng, W. Dong, R. Socher, L.-J. Li, K. Li, and L. Fei-Fei, “Imagenet: A large-scale hierarchical image database,” in *2009 IEEE conference on computer vision and pattern recognition*. Ieee, 2009, pp. 248–255.
- [33] Y. Seo, D. Hafner, H. Liu, F. Liu, S. James, K. Lee, and P. Abbeel, “Masked world models for visual control,” in *CoRL*, 2023.
- [34] C. Wang, X. Luo, K. Ross, and D. Li, “Vrl3: A data-driven framework for visual deep reinforcement learning,” *Advances in Neural Information Processing Systems*, 2022.
- [35] J. Schulman, F. Wolski, P. Dhariwal, A. Radford, and O. Klimov, “Proximal policy optimization algorithms,” *arXiv preprint arXiv:1707.06347*, 2017.
- [36] L. Yang, B. Kang, Z. Huang, X. Xu, J. Feng, and H. Zhao, “Depth anything: Unleashing the power of large-scale unlabeled data,” in *Proceedings of the IEEE/CVF conference on computer vision and pattern recognition*, 2024, pp. 10371–10381.
- [37] Z. Liu, H. Mao, C.-Y. Wu, C. Feichtenhofer, T. Darrell, and S. Xie, “A convnet for the 2020s,” 2022. [Online]. Available: <https://arxiv.org/abs/2201.03545>
- [38] P. J. Rousseeuw, “Silhouettes: a graphical aid to the interpretation and validation of cluster analysis,” *Journal of computational and applied mathematics*, vol. 20, pp. 53–65, 1987.
- [39] L. v. d. Maaten and G. Hinton, “Visualizing data using t-sne,” *Journal of machine learning research*, vol. 9, no. Nov, pp. 2579–2605, 2008.
- [40] R. R. Selvaraju, M. Cogswell, A. Das, R. Vedantam, D. Parikh, and D. Batra, “Grad-cam: Visual explanations from deep networks via gradient-based localization,” *International Journal of Computer Vision*, vol. 128, no. 2, p. 336–359, Oct. 2019. [Online]. Available: <http://dx.doi.org/10.1007/s11263-019-01228-7>
- [41] A. Dosovitskiy *et al.*, “An image is worth 16x16 words: Transformers for image recognition at scale,” *arXiv preprint arXiv:2010.11929*, 2020.
- [42] H. Chefer, S. Gur, and L. Wolf, “Transformer interpretability beyond attention visualization,” 2021. [Online]. Available: <https://arxiv.org/abs/2012.09838>